




One-proton removal from neutron-rich carbon isotopes in $^{12-16}\text{C}$ beams near 240 MeV/nucleon beam energy

Y. Z. Sun (孙亚洲) ¹, S. T. Wang (王世陶)^{1,2,*}, Z. Y. Sun (孙志宇) ^{1,2,†}, J. G. Li (李健国)¹, C. X. Yuan (袁岑溪) ³,
S. Y. Jin (金树亚)¹, X. H. Zhang (章学恒)¹, S. W. Tang (唐述文)¹, D. Yan (闫铎)¹, Y. H. Yu (余玉洪)¹,
F. Fang (方芳)¹ and Y. J. Zhang (张永杰)¹

¹*Institute of Modern Physics, Chinese Academy of Sciences, Lanzhou 730000, China*

²*School of Nuclear Science and Technology, University of Chinese Academy of Sciences, Beijing 100049, China*

³*Sino-French Institute of Nuclear Engineering and Technology, Sun Yat-Sen University, Zhuhai 519082, China*



(Received 18 April 2024; accepted 12 June 2024; published 1 July 2024)

The inclusive cross sections of one-proton removal from neutron-rich carbon isotopes $^{13-15}\text{C}$ on a carbon target near 240 MeV/nucleon were measured at the External Target Facility, HIRFL-CSR (Heavy Ion Research Facility in Lanzhou, Cooler Storage Ring). Together with the data for ^{12}C and ^{16}C at similar energies, the measurements are compared with Glauber model predictions weighted by spectroscopic strengths calculated by various shell models, namely standard shell model (SM), Gamow shell model (GSM), and no-core shell model (NCSM), which differ in the amount and aspects of included internucleon correlations. The dependencies of the spectroscopic strength reduction factor R_s on the binding depth ΔS of the removed proton are plotted. The obtained R_s - ΔS relations of GSM and SM turn out to be largely consistent with the earlier-observed systematics, whereas the NCSM R_s exhibit an appreciable overall increase. GSM and NCSM predictions both compare better with experiment than SM and tend to alleviate the odd-even staggering of R_s against projectile mass number A . The R_s of ^{15}C is intriguingly large compared with the rather low R_s of ^{16}C , for which the reason is discussed.

DOI: [10.1103/PhysRevC.110.014603](https://doi.org/10.1103/PhysRevC.110.014603)

I. INTRODUCTION

The prohibitive mathematical difficulty in many-body problems of atomic nuclei and the complexity of the nature of the nuclear force call for an approximative treatment that involves solving the nucleus in an effective potential among the constituent nucleons in a truncated model space. The success of the independent particle model (IPM) [1] confirms the significance of a mean field in nuclei. With the inclusion of residual interactions between nucleons in addition to the mean field, IPM has evolved into modern shell models that have advanced their applicability to nuclei lying far off the β -stability valley of the nuclear chart [2]. Shell models solve the wave function of a nucleus by diagonalizing the Hamiltonian matrix in a truncated model space, leading to configuration mixing and fragmented shell occupancies of valence nucleons that spread over orbits above the Fermi level. The comparison of experimental measurements of the occupancies with theoretical predictions provides valuable evaluations for the structural models and in turn advances our understanding of internucleon correlations in exotic nuclei.

Radioactive ion beams (RIBs) are widely employed to extract the shell occupancy of valence nucleons in short-lived nuclei [3], by means of, e.g., one-nucleon knockout reactions.

Accordingly, the shell occupancy of the removed nucleon is represented by spectroscopic factor C^2S between the projectile ground state (g.s.) and the valence configuration of the bound mass $A - 1$ residue (core) final state + the valence nucleon orbit, expressed as [3]

$$\langle \mathbf{r}, \Psi_{\alpha}^{A-1} | \Psi_{\text{g.s.}}^A \rangle = \sum_{nlj} c_{nlj,\alpha} \psi_{nlj}(\mathbf{r}),$$

$$C^2S(\alpha, nlj) = |c_{nlj,\alpha}|^2, \quad (1)$$

where \mathbf{r} is the coordinate of the valence nucleon, and α denotes the final state of the core. The spectroscopic factors enter the calculation of inclusive single-nucleon removal cross section via [4]

$$\sigma_{\text{th}} = \sum_{\alpha, nlj} \left(\frac{A}{A-1} \right)^N C^2S(\alpha, nlj) \sigma_{\text{sp}}(nlj, S_{\alpha}^*). \quad (2)$$

where σ_{sp} is the so-called single-particle (sp) cross section calculated by the Glauber reaction model [5] assuming that $|\Psi_{\text{g.s.}}^A\rangle$ has only one valence configuration (α, nlj) and $C^2S(\alpha, nlj) = 1$. The $[A/(A-1)]^N$ factor is a center-of-mass correction [6], and $N = 2n + l = 0, 1, 2, \dots$ the major oscillator quanta of the valence nucleon's orbit. $S_{\alpha}^* = S_{n(p)} + E_{\alpha}^*$ is the effective nucleon separation energy with regard to (w.r.t.) the core state α , where $S_{n(p)}$ is the ground-state-to-ground-state separation energy of the valence neutron (proton), and E_{α}^* is the energy of the core state α w.r.t. its ground state. The

*Contact author: wangshitao@impcas.ac.cn

†Contact author: sunzhy@impcas.ac.cn

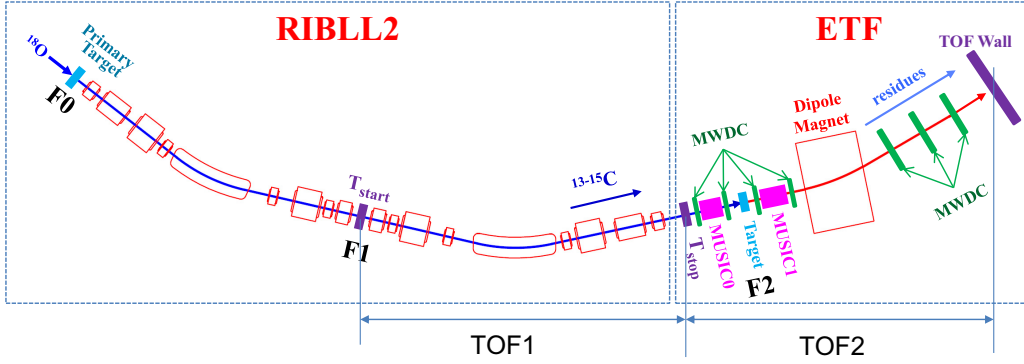


FIG. 1. A schematic view of RIBLL2 and ETF. The flight paths of TOF1 and TOF2 are also marked.

sum runs over all the valence configurations (α, nlj) to give the bound-core inclusive cross section.

There is a universal and longstanding overestimation of inclusive cross sections of single-nucleon removal on composite (usually carbon or beryllium) target since it was first compiled in Ref. [7] and later updated in Refs. [8,9]. Defining a reduction factor [7]

$$R_s \equiv \frac{\sigma_{\text{exp}}}{\sigma_{\text{th}}}, \quad (3)$$

where σ_{exp} is the experimental counterpart of σ_{th} , it is found that the existing data portrait a picture where R_s drops almost linearly w.r.t the binding depth (represented by ΔS ; see Ref. [8] or Sec. V for a definition) of the removed nucleon, ranging from nearly unity to as low as around 0.25 [9].

While it is well understood that the overestimation for stable nuclei originates from internucleon correlations beyond that accounted for in shell models, the reason for the R_s - ΔS dependence is not clear [10], which may originate from deficiencies in both structure theories and reaction models. Since the Glauber model builds upon the sudden (fast collision) and eikonal (forward scattering) approximation (SE approximation), high beam energies (E_b) enhance its validity. In addition to the data mainly in the range 80–120 MeV/nucleon from the original compilation [7], the growing data with E_b around 240 MeV/nucleon [9,11] and higher [12] in recent publications find no considerable E_b dependence of R_s - ΔS systematics. Besides, the destruction of the mass $A - 1$ core in indirect processes is not accommodated in the Glauber model, which may contribute significantly to the severe overestimation of deeply bound nucleon removal [13,14]. While direct measurements of the core destruction are still scarce, investigations on structural calculations are drawing more attention. A recent study on partial cross sections of one-nucleon removal to the ground state of the core observed a much flatter R_s - ΔS scatter plot than described above; it treats the effects of short- and long-range NN correlations with no explicit truncation on the basis of available configurations by using variational Monte Carlo (VMC) many-body calculations [15].

To further confirm the high incident energy behavior of R_s w.r.t. ΔS , and study the contribution of missing correlations in shell models to it, we have conducted a consistent measurement of single-proton removal from a series of neutron-rich carbon isotopes $^{12-16}\text{C}$ near 240 MeV/nucleon. The $^{12,16}\text{C}(-p)$ data have been published in Refs. [16,17],

respectively. We have updated the $^{16}\text{C}(-p)$ cross section [from 16(2) to 18.2(20) mb] with an improved tracking algorithm [18] in this work, and quoted the ^{12}C one.

The R_s - ΔS plot is extracted and discussed. State-of-the-art theoretical models, i.e., the *ab initio* no-core shell model (NCSM [19,20]) and Gamow shell model (GSM [21,22]), are employed to interpret the experiment data for comparison with the standard shell model (SM) calculations.

II. EXPERIMENT

The experiment was performed at the External Target Facility (ETF [23]) at the Heavy Ion Research Facility in Lanzhou (HIRFL [24]). Primary ^{18}O beams were accelerated in the main Cooler Storage Ring (CSRm [25]) to 280 MeV/nucleon and steered off the ring to be fragmented on a 15-mm-thick beryllium target. The produced secondary beams were then selected by their magnetic rigidities in the second Radioactive Ion Beam Line in Lanzhou (RIBLL2 [26]) and delivered to ETF to impinge on a 5-mm-thick carbon target. The mid-target energies for the $^{12,13,14,15,16}\text{C}$ beams were 230, 234, 235, 237, and 239 MeV/nucleon, respectively. A schematic view of the experiment setup of RIBLL2 and ETF is given in Fig. 1.

The secondary beams are identified from their Z - A/Z spectra, where the charge number Z is deduced from the beams' energy deposit ΔE measured by the MULTI-Sampling Ionization Chamber 0 (MUSIC0 [27]), and the mass-over-charge ratio A/Z is given by the time of flight (TOF) in RIBLL2 (TOF1 in Fig. 1) measured by plastic scintillators T_{start} [28] and T_{stop} [29]. The secondary beams are clearly separated, as seen in Fig. 2, for the particle identification (PID) spectrum under the ^{14}C setting of RIBLL2. The beam intensities for $^{12,13,14,15,16}\text{C}$ are around 100, 90, 320, 140, and 150 particles per second, respectively.

PID of the heavy reaction residues is achieved via $B\rho$ - ΔE -TOF method. A/Z of the residues are calculated according to

$$B\rho \propto p/Z \propto (A/Z)\beta\gamma, \quad (4)$$

where ρ is the radius of the particle trajectory in the dipole magnet (see Fig. 1) deduced from the tracks recorded by the multiwire drift chambers (MWDCs) upstream [23] and downstream [30] of the dipole magnet. p is the momentum

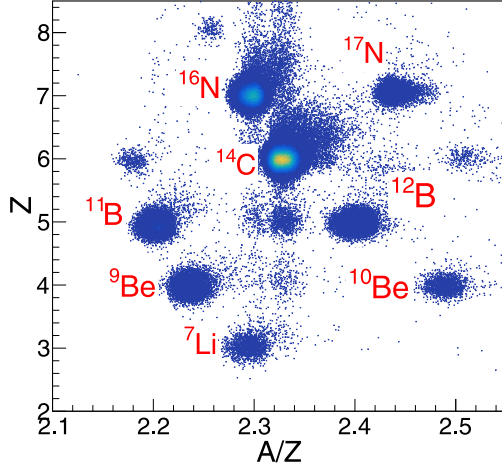


FIG. 2. The PID spectrum of the secondary beams under RI-BLL2's ^{14}C setting.

of the residues. β and γ are the corresponding velocity and Lorentz factor, extracted from TOF2 (see Fig. 1) measured by plastic scintillators T_{stop} [29] and the TOF wall [31]. Details about the tracking method and the PID method of the residues are found in Refs. [18,30] and [23], respectively. Similarly, the charge numbers Z of the residues were given by their energy deposit ΔE_1 in ionization chamber MUSIC1 [32]. Figure 3 presents the PID spectrum of the reaction residue of the ^{14}C beam, from which it is seen that ^{13}B is clearly separated. The upgoing tail of ^{14}C is attributed to pileup of MUSIC1. The horizontal tails are caused by tracking deficiency (contributing to tails on both sides) and particles that skimmed over the surface of the TOF wall strips [31], which introduced delay to the timing of the hit (contributing only to the tail on the right side).

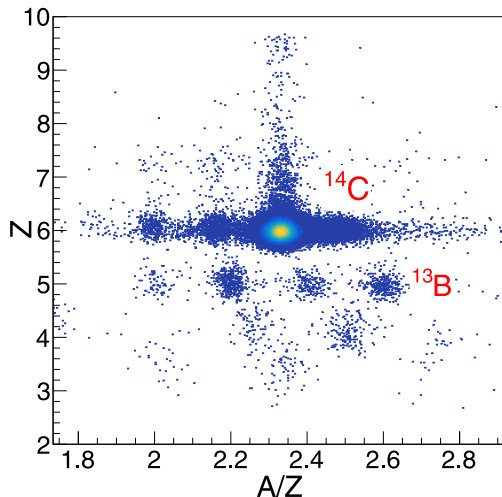


FIG. 3. PID spectrum of the reaction residues of $235\text{ MeV/nucleon }^{14}\text{C}$ impinging on a carbon target.

III. DATA ANALYSIS

The cross section for a certain reaction channel i is calculated using

$$\sigma_i = \frac{\Delta N_i}{N_0 t \epsilon}, \quad (5)$$

where N_0 and ΔN_i are the counts of the projectile and the objective products. t is the number of target nuclei per area, and ϵ the correction for N_i , including detecting efficiency, geometrical efficiency and loss in the 5-mm-thick target [11]. Position distribution reconstructed from MWDC Array 1 shows that the geometrical acceptance for $-p$ products of all the considered carbon beams are $\approx 100\%$. The detection efficiency ϵ_d is defined as the probability that an outgoing particle from the secondary target successfully passes through the sensitive areas of all the detectors and is identified. The ϵ_d for boron residues are evaluated to be around 88% by using the boron secondary beams in target-out runs [33].

The $-p$ product is selected in the PID spectrum by an ellipse with its axes being $a = 3\sigma_{A/Z}$ and $b = 3\sigma_Z$, where $\sigma_{Z(A/Z)}$ is the σ of a Gaussian fit to the $Z(A/Z)$ distribution. Contribution to the cross section from reactions happened other than on the reaction target is estimated from target-out runs and subtracted. The extracted cross sections for the $-p$ channel for the carbon beams are listed in Table I.

IV. THEORETICAL CALCULATIONS

The theoretical inclusive $-p$ cross sections are calculated according to Eq. (2). The single-particle cross section σ_{sp} is computed within the Glauber model formalism [34–36] following techniques similar to those detailed in Ref. [7]. The valence proton-core relative wave functions $|\psi_{nlj}\rangle$ are solved in a Woods-Saxon (WS) potential plus spin-orbit and Coulomb terms. The depths V_0 and radius r_0 of the central WS potentials are determined so that the resulting $|\psi_{nlj}\rangle$ reproduces the effective nucleon separation energy S_α^* and the root-mean-square (rms) radius of the valence proton given by Hartree-Fock (HF) calculations using SkX parametrization [37]. This procedure is implemented for each valence configuration (α, nlj) , with bound states α of the boron residues collected from online database NuDat3 [38]. The spin-orbit potentials use a fixed depth $V_{\text{so}} = 6\text{ MeV}$ and r_0 fitted from above. A diffuseness parameter of $a = 0.7\text{ fm}$ is applied throughout. The t - ρ - ρ approximation [5,35,36] is adopted to construct the elastic scattering S matrices of the valence proton and the core with the target, where the nucleon densities of the target and the core are needed. The latter are given by the aforementioned HF calculations. A Gaussian density with rms radius of 2.32 fm is assumed for the nucleon density of the target. Following Ref. [39], we have assumed a Gaussian effective interaction with range parameter $\beta_{mn} = \beta_{pn} = 0.5\text{ fm}$ for the NN scattering amplitude $f_{NN}(q)$.

As mentioned in the Introduction, spectroscopic factors C^2S are calculated from three species of shell models which differ in the amount and aspect of incorporated NN correlations. The SM calculations are implemented with active

TABLE I. The inclusive $-p$ cross sections of $^{12-16}\text{C}$ on a carbon target. $(I_c^\pi E_\alpha^*, nlj)$ specifies the valence configuration with bound core state α and valence proton orbit nlj . r_{HF} is the rms radius of the valence proton from HF calculations. $\Delta S = S_p + \bar{E}^* - S_n$ defines the binding depth of the valence proton, where \bar{E}^* is the averaged core excitation energy weighted by the partial cross sections of core state α to the total cross section σ_{th} . $R_s = \sigma_{\text{exp}}/\sigma_{\text{th}}$ are the reduction factor of spectroscopic factors. The incident energies E_k are in MeV/nucleon.

Projectile	E_k (MeV/nucleon)	σ_{exp} (mb)	nlj	I_c^π	E_α^* (MeV)	σ_{sp} (mb)	C^2S^{SM}	C^2S^{GSM}	C^2S^{NCSM}	R_s^{SM}	R_s^{GSM}	R_s^{NCSM}
^{12}C	230		$0p_{1/2}$	$1/2^-$	2.125	21.33	0.7229	0.2442	0.6096			
			$0p_{3/2}$	$3/2_1^-$	0	22.56	2.8594	3.2667	2.7385			
				$3/2_2^-$	5.020	20.34	0.1548	0.3730	0.0869			
	Inclusive	63.9(66) [17]					3.7371	3.8849	3.4349	0.71(7)	0.68(7)	0.83(9)
^{13}C	234		$0p_{1/2}$	1^+	0	20.42	0.1080	0.0001	0.0046			
			$0p_{1/2}$	0^+	2.723	19.34	0.1424	0.0490	0.1088			
			$0p_{3/2}$	1^+	0	20.59	1.0775	1.1157	1.0840			
			$0p_{3/2}$	2^+	0.953	20.16	1.9888	1.9021	1.8796			
	Inclusive	39.5(60)					3.2287	3.0669	3.0770	0.56(8)	0.58(9)	0.63(10)
^{14}C	235		$0p_{1/2}$	$1/2^-$	3.713	16.81	0.1852	0.2245	0.1141			
			$0p_{3/2}$	$3/2_1^-$	0	18.12	3.5146	3.0142	3.3002			
	Inclusive	41.3(27)					3.6998	3.2387	3.4142	0.57(4)	0.66(4)	0.67(4)
^{15}C	237		$0p_{3/2}$	2^-	0	16.80	1.6084	1.8122	1.5185			
			$0p_{3/2}$	1^-	0.654	16.58	1.1651	1.0911	1.1299			
	Inclusive	28.4(28)					2.7735	2.9033	2.6483	0.57(6)	0.55(5)	0.64(6)
^{16}C	239		$0p_{3/2}$	$3/2^-$	0	17.45	2.8476	2.4052	2.2656			
	Inclusive	18.2(20)					2.8476	2.4052	2.2656	0.34(4)	0.41(4)	0.46(5)

nucleons in the p - sd shell using WBP interaction [40], assuming an inert α core.

Moreover, the GSM [21,22] and *ab initio* NCSM [19,20] are also employed to calculate the C^2S , and to compare with the results of SM calculations. Contrary to the standard SM in which the calculations are performed within a limited model space using an inner frozen core, the NCSM calculations are done without assuming an inner core, and all the valence nucleons are active and treated on an equal footing. The nucleon-nucleon Daejeon16 interaction [41], which provides appropriate descriptions for light nuclei, is adopted in the present work to calculate the C^2S for the C isotopes. The N_{max} is used for model space truncation in the real calculations. For the nuclei investigated in the present work, $N_{\text{max}} = 6$ is adopted. Following Ref. [42], the center-of-mass correction in Eq. (2) is not applied to NCSM calculations.

GSM is usually performed in the picture of a core plus valence particles, which is similar to the standard shell model calculations. The fundamental theoretical construction entering GSM is the one-body Berggren basis [43], which consists of bound, resonance, and scattering sp states. However, only the bound sp states are used in standard SM calculations. From the Berggren basis, a many-body basis of Slater determinants can be generated, so that internucleon correlations are described via configuration mixing [21,22,44,45]. The internucleon correlations and continuum coupling are well treated within the GSM calculations. Hence, GSM is a suitable approach to studying weakly bound and unbound states. In the real calculations for the C^2S of the C isotopes, we performed the GSM calculation above the ^8He inner core using the nucleon-nucleon Minnesota interaction [46]. The valence neutrons are active within a model space which consists of s , $p_{3/2,1/2}$, and $d_{5/2}$ partial waves within Berggren basis, and $d_{3/2}$ partial waves within harmonic oscillator (HO) basis. For the

valence protons, the model space is chosen as $p_{3/2,1/2}$ within Berggren basis and $s_{1/2}$ waves with HO basis.

V. RESULTS AND DISCUSSION

The C^2S and σ_{sp} for each valence configuration of all the projectiles are tabulated in Table I, together with the eventual R_s using SM, NCSM, and GSM structural inputs. The binding depth ΔS of the removed proton is defined as $\Delta S = S_p + \bar{E}^* - S_n$, where \bar{E}^* is the averaged core excitation energy weighted by the contribution to σ_{th} from each valence configuration.

With the data in Table I, an R_s - ΔS scatter plot is drawn in Fig. 4, over a hatched band summarizing the totality of the R_s - ΔS systematics given in Fig. 1 of Ref. [9], compiled from data with beam energies mainly in the range 80–240 MeV/nucleon. The data points of SM and GSM (NCSM) are put together in Fig. 4(a) [Fig. 4(b)] to facilitate comparison, with linear fits to each data set superimposed. The fitted lines for SM, GSM, and NCSM are $R_s = -0.0136(36)\Delta S + 0.698(57)$, $R_s = -0.0104(35)\Delta S + 0.698(56)$, and $R_s = -0.0138(43)\Delta S + 0.808(66)$, respectively, in contrast with $R_s = -0.016\Delta S + 0.61$ in Ref. [9].

Figure 4 shows that, despite the differences in the structural models, all the three datasets largely follow the formerly established R_s - ΔS systematics, and agree with each other pretty well in the slope of the trend. In contrast with the much flatter trend in Ref. [15], it appears that both NCSM and GSM fail to grab the dominant part of the missing NN correlations in the shell models that may significantly mitigate the binding depth dependence of the spectroscopic strength quenching.

Nevertheless, it is still a promising start. The NCSM R_s values are all augmented w.r.t. their SM counterparts considerably towards unity, which gives rise to a systematic upward

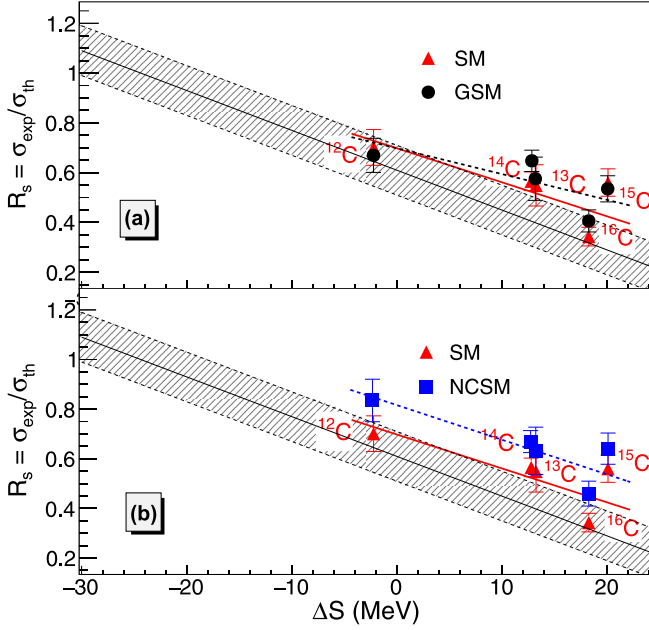


FIG. 4. The R_s - ΔS plot for one-proton removal from $^{12-16}\text{C}$ near 240 MeV/nucleon. Panels (a) and (b) correspond to the comparisons of results using structural input from SM vs GSM and SM vs NCSM, respectively. In each figure, the hatched band summarizes the totality of the R_s - ΔS systematics from Fig. 1 of Ref. [9]. The solid line is a linear fit to the SM data points, while the dashed line is that for GSM or NCSM.

deviation from the hatched band, as is clearly reflected by the fitted lines. This may originate from the differences in the interactions used in the two models, and/or core (the inert core frozen by SM) excitation during the proton removal.

Due to the ^8He core used in the GSM calculations, R_s of ^{12}C from GSM may be underestimated, as only two valence protons and no valence neutron are active. Apart from ^{12}C , a trend of general R_s augmentation similar to that of NCSM is seen in GSM results with the exception of ^{15}C , which is discussed below.

The disparate data of ^{15}C and ^{16}C draw special attention. Both of them deviate from the corresponding linear fits considerably in all circumstances in Fig. 4. The R_s of ^{15}C is abruptly large, given its ΔS value. It makes the case even more bewildering as ^{15}C is a weakly bound nuclei with a well-known $1s$ -orbit one-neutron halo [3,47] and $S_n = 1.2181$ MeV. There is evidence that the g.s. of residue ^{14}B also possesses a halo-like neutron in the $1s$ orbit [48–50] with $S_n = 0.9695$ MeV, resembling its mother ^{15}C . It appears that the removal of a deeply bound proton from ^{15}C will leave the residual ^{14}B susceptible to breakup via indirect processes so as to decrease the $-p$ cross section and change the R_s in the opposite direction, in contradiction with our results. It is noteworthy that the optical limit (or static density) approximation of Glauber model calculations (as manifested in the t - ρ - ρ approximation adopted in this work) tends to overestimate the reaction cross section of halo nuclei [51,52]. A recent study shows that this has negligible effects on the calculated deeply bound nucleon removal cross section, leading to a

TABLE II. Relative increase of R_s of GSM and NCSM w.r.t. SM, quantified by $\varepsilon^X \equiv (R_s^X - R_s^{\text{SM}})/R_s^{\text{SM}} = (\sigma_{\text{th}}^X - \sigma_{\text{th}}^{\text{SM}})/\sigma_{\text{th}}^{\text{SM}}$, where X is GSM or NCSM.

Projectile	^{13}C	^{14}C	^{15}C	^{16}C
ε^{GSM}	0.050	0.144	-0.045	0.184
$\varepsilon^{\text{NCSM}}$	0.135	0.166	0.122	0.341

weakly bound residue [15] by comparison with calculations using few-body model S matrices for the residue [53]. Indirect processes are not yet explicitly included in the Supplemental Material [53] of Ref. [15]. Given the resemblance in halo structure of ^{15}C and ^{14}B , a lowered R_s of ^{15}C from GSM is expected, as GSM is a tuned shell model for description of weakly bound nuclei [21], which is supposed to reflect the resemblance and produce enhanced C^2S to argument σ_{th} . Since this decrease is marginal as shown in Fig. 4, the large R_s of ^{15}C still awaits an explanation.

The odd-even staggering (OES) of R_s w.r.t. projectile mass number A in one-nucleon removal was observed in Ref. [12], where R_s of even- A is much lower from the systematics than odd- A , for which the Authors suggest its cause as more structure-related than reaction-related. OES is not so pronounced in Fig. 4. In fact, we observe appreciable enhancements for R_s of even- A projectiles compared with odd- A ones, which tends to flatten the OES, as shown in Table II. Since the difference is caused by different treatments in shell models, this further hints a structural origin of the OES.

VI. CONCLUSIONS

Inclusive cross sections of one-proton removal from $^{13-15}\text{C}$ near 240 MeV/nucleon on a carbon target are measured and compared with Glauber model predictions using spectroscopic factors C^2S calculated from the standard shell model, Gamow shell model, and no-core shell model. The reduction factors R_s of the spectroscopic factors are deduced, and plotted against the binding depth ΔS of the removed proton. The R_s - ΔS dependence using SM, GSM, and NCSM structural inputs largely follow the previously observed systematics, indicating that the majority of the missing NN correlation beyond that accounted for in SM is still not incorporated in GSM or NCSM. The σ_{th} of GSM and NCSM agree better with experiment than SM in that NCSM ones and most of GSM ones have generally smaller deviations from σ_{exp} . SM, GSM, and NCSM data all show an intriguingly large R_s of ^{15}C , given the large ΔS value and weakly bound nature of the residual ^{14}B . Our work is in favor of a structural origin of odd-even staggering of R_s w.r.t. projectile mass number A .

ACKNOWLEDGMENTS

The authors are obliged to the crew of HIRFL-CSR and the External Target Facility for providing high-quality secondary beams. We wish to thank Prof. J. A. Tostevin for the Glauber-

model calculations of the single-particle cross sections. This work was supported by the National Natural Science Foundation of China (Grant No. 12305133), the Open Research

Project of CAS Large Research Infrastructures, China Postdoctoral Science Foundation (Grant No. 2023M733575), and Longyuan Youth Talent Program.

-
- [1] M. G. Mayer, *Phys. Rev.* **75**, 1969 (1949).
[2] E. Caurier, G. Martinez-Pinedo, F. Nowack, A. Poves, and A.P. Zuker, *Rev. Mod. Phys.* **77**, 427 (2005).
[3] P. G. Hansen and J. A. Tostevin, *Annu. Rev. Nucl. Part. Sci.* **53**, 219 (2003).
[4] C. Wen *et al.*, *Chin. Phys. C* **41**, 054104 (2017).
[5] C. A. Bertulani and P. Danielewicz, *Introduction to Nuclear Reactions* (Institute of Physics, Bristol, 2004), p. 428.
[6] A. E. L. Dieperink and T. de Forest, *Phys. Rev. C* **10**, 543 (1974).
[7] A. Gade *et al.*, *Phys. Rev. C* **77**, 044306 (2008).
[8] J. A. Tostevin and A. Gade, *Phys. Rev. C* **90**, 057602 (2014).
[9] J. A. Tostevin and A. Gade, *Phys. Rev. C* **103**, 054610 (2021).
[10] T. Aumann *et al.*, *Prog. Part. Nucl. Phys.* **118**, 103847 (2021).
[11] Y. Z. Sun *et al.*, *Phys. Rev. C* **104**, 014310 (2021).
[12] Y. Z. Sun *et al.*, *Phys. Rev. C* **106**, 034614 (2022).
[13] C. Louchart, A. Obertelli, A. Boudard, and F. Flavigny, *Phys. Rev. C* **83**, 011601(R) (2011).
[14] Y. L. Sun *et al.*, *Phys. Rev. C* **93**, 044607 (2016).
[15] A. N. Kuchera *et al.*, *Phys. Rev. C* **105**, 034314 (2022).
[16] Y. X. Zhao *et al.*, *Phys. Rev. C* **100**, 044609 (2019).
[17] B. Mei *et al.*, *Phys. Rev. C* **108**, 034602 (2023).
[18] Y. Z. Sun *et al.*, *Nucl. Instrum. Methods Phys. Res., Sect. A* **985**, 164682 (2021).
[19] P. N. Bruce, R. Barrett, and J. P. Vary, *Prog. Part. Nucl. Phys.* **69**, 131 (2013).
[20] J. G. Li, C. A. Bertulani, and F. R. Xu, *Phys. Rev. C* **105**, 024613 (2022).
[21] J. Li *et al.*, *Physics* **3**, 977 (2021).
[22] N. Michel and M. Płoszajczak, *The Gamow Shell Model: The Unified Theory of Nuclear Structure and Reactions* (Springer, Berlin, 2021), p. 428.
[23] Y. Z. Sun *et al.*, *Nucl. Instrum. Methods Phys. Res., Sect. A* **927**, 390 (2019).
[24] W. L. Zhan *et al.*, *Nucl. Phys. A* **805**, 533c (2008).
[25] J. W. Xia *et al.*, *Nucl. Instrum. Methods Phys. Res. Sect. A* **488**, 11 (2002).
[26] B. H. Sun *et al.*, *Sci. Bull.* **63**, 78 (2018).
[27] X. H. Zhang *et al.*, *Nucl. Instrum. Methods Phys. Res. Sect. A* **795**, 389 (2015).
[28] X. H. Zhang *et al.*, IMP & HIRFL Annual Report, **2013**, 217.
[29] W. J. Lin *et al.*, *Chin. Phys. C* **41**, 066001 (2017).
[30] Y. Z. Sun *et al.*, *Nucl. Instrum. Methods Phys. Res. Sect. A* **894**, 72 (2018).
[31] Y. Sun *et al.*, *Nucl. Instrum. Methods Phys. Res. Sect. A* **893**, 68 (2018).
[32] K. Kimura *et al.*, *Nucl. Instrum. Methods Phys. Res., Sect. A* **538**, 608 (2005).
[33] Y. Z. Sun *et al.*, *Nucl. Phys. Rev.* **37**, 742 (2020).
[34] J. A. Tostevin, *Nucl. Phys. A* **682**, 320 (2001).
[35] C. A. Bertulani and A. Gade, *Comput. Phys. Commun.* **175**, 372 (2006).
[36] Y. Z. Sun and S. T. Wang, *Comput. Phys. Commun.* **288**, 108726 (2023).
[37] B. A. Brown, *Phys. Rev. C* **58**, 220 (1998).
[38] NuDat 3.0, <https://www.nndc.bnl.gov/nudat3/>, accessed 11 Mar, 2024.
[39] B. A. Brown, P. G. Hansen, B. M. Sherrill, and J. A. Tostevin, *Phys. Rev. C* **65**, 061601(R) (2002).
[40] E. K. Warburton and B. A. Brown, *Phys. Rev. C* **46**, 923 (1992).
[41] A. M. Shirokov *et al.*, *Phys. Lett. B* **761**, 87 (2016).
[42] G. F. Grinyer *et al.*, *Phys. Rev. Lett.* **106**, 162502 (2011).
[43] T. Berggren, *Nucl. Phys. A* **109**, 265 (1968).
[44] N. Michel, W. Nazarewicz, M. Płoszajczak, and K. Bennaceur, *Phys. Rev. Lett.* **89**, 042502 (2002).
[45] M. R. Xie *et al.*, *Phys. Lett. B*, **839** 137800 (2023).
[46] D. R. Thompson, M. Lemere, and Y. C. Tang, *Nucl. Phys. A* **286**, 53 (1977).
[47] J. Al-Khalili, *Lect. Notes Phys.* **651**, 77 (2004).
[48] M. Fukuda *et al.*, *EPJ Web Conf.* **66**, 02037 (2014).
[49] V. Guimarães *et al.*, *Phys. Rev. C* **61**, 064609 (2000).
[50] E. Sauvan *et al.*, *Phys. Lett. B* **491**, 1 (2000).
[51] J. S. Al-Khalili and J. A. Tostevin, *Phys. Rev. Lett.* **76**, 3903 (1996).
[52] R. C. Johnson and C. J. Goebel, *Phys. Rev. C* **62**, 027603 (2000).
[53] The Supplemental Material of Ref. [15], <http://link.aps.org/supplemental/10.1103/PhysRevC.105.034314>, 2022, accessed 11 Mar, 2024.